Electronic supplementary information

Synergistic photothermal-dual site strategy to accelerate proton–electron transfer enables enhanced CO_2-to-syngas conversion.

Lang Pei,[1,2*] Haichuan Feng,[1] Qinan Mao,[1] Lixiang Wang,[1] Yu Zhang,[1] Xin Wen,[3*] Xusheng Wang,[4] Xiao Liu[5*]

[1] College of Materials and Environmental Engineering, Hangzhou Dianzi University, Hangzhou 310018, China

[2] Laboratory of Solid State Microstructures, Nanjing University, Nanjing 210093, China

[3] Guangxi Key Laboratory of Information Materials, Guangxi Collaborative Innovation Center of Structure and Property for New Energy and Materials, School of Materials Science and Engineering, Guilin University of Electronic Technology, Guilin 541004, China

[4] School of Materials Science and Engineering, Zhejiang Sci-Tech University, Hangzhou 310018, China

[5] Institute of Carbon Neutrality and New Energy, School of Electronics and Information, Hangzhou Dianzi University, Hangzhou 310018, China

[*]**E-mail: peilang@hdu.edu.cn; wenxin@guet.edu.cn; liuxiao@hdu.edu.cn**

1.1 Materials characterization:

Scanning electron microscopy (SEM) was conducted using a JEOL-JSM-IT300HR field emission microscope. Transmission electron microscopy (TEM) and elemental mapping were performed with a JEOL-2010 TEM operating at an acceleration voltage of 200 kV. The molar ratio of Pt to Ta was determined by inductively coupled plasma-optical emission spectroscopy (ICP-OES) using an Optima 5300DV instrument (Perkin Elmer). X-ray diffraction (XRD) patterns were acquired with a Rigaku Ultima III X-ray diffractometer utilizing Cu Kα radiation. Electron paramagnetic resonance (EPR) spectra were obtained at room temperature (25 °C) employing a Bruker A300-10/12 EPR spectrometer. X-ray photoelectron spectroscopy (XPS) measurements were performed using a Ka X-ray photoelectron spectrometer (Thermo Scientific), where the binding energy was calibrated to the C 1s peak at 284.6 eV as a charge reference. Light absorption spectra were recorded with a UV-vis spectrophotometer (UV-2450, Shimadzu Co., Japan). The H_2O temperature-programmed desorption (TPD) spectroscopy was conducted on a Micromeritics AutoChem II chemisorption analyzer connected to a Pfeiffer OmniStar mass spectrometer. In-situ Fourier transform infrared (FTIR) spectroscopy was performed using a Nicolet Nexus 870 infrared spectrometer (Nicolet, USA). Photoluminescence (PL) spectra were acquired with a fluorescence spectrometer (Edinburgh Instrument FS5). Photoelectrochemical measurements were carried out in a standard three-electrode setup utilizing a CHI 660E electrochemical workstation (Chenhua, China). The electrolyte was N_2-saturated 1M NaOH, with a Pt foil serving as the counter electrode and a Hg/HgO electrode as the reference. The prepared samples were spin-coated onto fluorine-doped SnO_2 (FTO) glass at 500 rpm for 30 s, functioning as self-supported working electrodes. Electrode potentials were converted to the reversible hydrogen electrode (RHE) reference scale using $E_{RHE} = E_{Hg/HgO} + 0.098\ V + 0.059 * pH$. The EIS curved were tested at open-circuit voltage (OCV) from 0.01 Hz to 10 MHz with a sinusoidal voltage amplitude of 5.0 mV.

1.2 Apparent Quantum Yield Calculation

The AQY test of 0.5Pt/Ta_2O_{5-x} was taken under constant 8 h irradiation by a 300 W xenon lamp with a monochromator (λ =365 nm) band-pass filter (ZBPA500, Asahi Spectra Co., FWHM: 10 nm). The average light intensity was recorded to be 10 mW cm^{-2} by a spectroradiometer and the irradiation area was 4.2 cm^2. The amount of incident electrons (N) is determined by equation:

$$N = \frac{E \times S \times t \times \lambda}{h \times c} = \frac{10 \times 10^{-3} \times 4.2 \times 8 \times 3600 \times 365 \times 10^{-9}}{6.626 \times 10^{-34} \times 3 \times 10^{8}}$$

$$= 2.22 \times 10^{21} \qquad (1)$$

The amount of CO and H_2 molecule yielded at 8 h was 15.6 μmol and 49.3 μmol, respectively. The AQY was calculated by equation:

$$AQY = \frac{2 \times number\ of\ (CO + H_2) moleculer}{number\ of\ incident\ photons} \times 100\%$$

$$= \frac{2 \times (15.6 + 49.3) \times 10^{-6} \times 6.02 \times 10^{23}}{2.22 \times 10^{21}} \times 100\%$$

$$= 3.5\% \qquad (2)$$

where E, S, t, λ, h, and c are the average light intensity (10 mW cm^{-2} nm^{-1}), the illumination area (4.2 × cm^2), the illumination time (8 × 3600 s), the wavelength of the incident light (365 × 10^{-9} m), the Planck constant (6.626 × 10^{-34} J·s) and the velocity of light (3 × 10^8 m s^{-1}), respectively

1.3 Theoretical calculations

All the calculations were carried out based on density functional theory (DFT) with the Perdew-Burke-Ernzerbof (PBE) form of generalized gradient approximation

functional (GGA) by employing the Vienna ab-initio simulation package (VASP).[1-3] The Blöchl's all-electron-like projector augmented wave (PAW) method was used to describe the interactions between valence electrons and ion cores. [4] To construct the composite model of Pt/Ta_2O_{5-x}, the (001) surface of Ta_2O_{5-x} with four atomic layers and the Pt cluster with eight Pt atoms are employed, where a 1.5 nm vacuum layer was added to avoid interactions. To reduce the lattice mismatch between Ta_2O_{5-x}(001) surface and Pt cluster, a 2×2 supercell of Ta_2O_{5-x}(001) are chosen. The lattice parameters of Ta_2O_{5-x} were calculated first with the plane wave cutoff energy set as 500 eV and the k-point mesh set as 8 × 12 × 6. To calculate the Ta_2O_{5-x}(001) slab, a 2 × 2 supercell is created and a 20 Å vacuum layer is added on top of the supercell to avoid inter-layer interactions. The oxygen vacancy on the Ta_2O_{5-x}(001) slab was created by removing one surface O atom from the perfect Ta_2O_5(001) surface. The free energies of adsorption are then calculated as $\Delta G=\Delta E_{DFT}+E_{ZPE}-TS$, where ΔE_{DFT}, E_{ZPE}, T, and S are adsorption enthalpy, zero-point energy, temperature (300 K), and entropy, respectively. Standard ideal gas methods were employed to compute E_{ZPE} and TS from temperature, pressure and the calculated vibrational energies. The limiting potential is calculated by taking the negative of the maximum free energy difference between each two successive steps in the free energy diagram. The computational hydrogen electrode model was employed to assess the free energy changes for each reaction step that involves a proton–electron pair transfer. In this model, the free energy of a proton-electron pair at 0 V vs. RHE is equivalent to half the free energy of a hydrogen molecule.

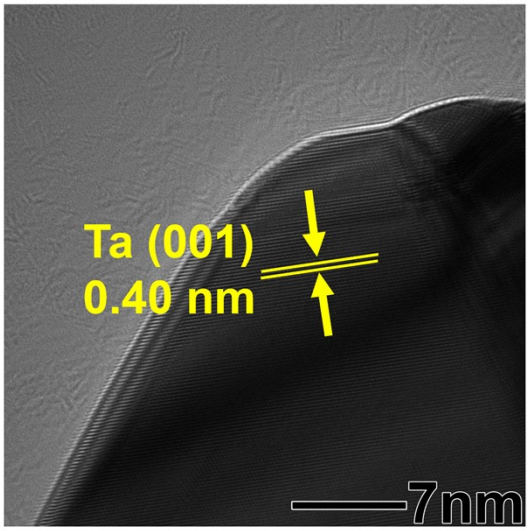

Fig. S1. The HRTEM image of Ta_2O_{5-x}.

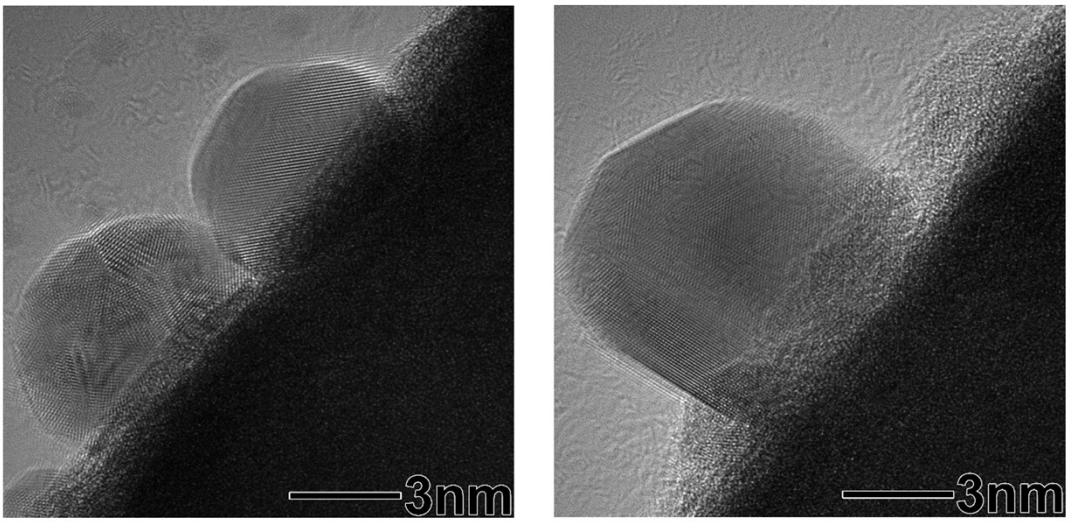

Fig. S2. The HRTEM images of $0.5Pt/Ta_2O_{5-x}$.

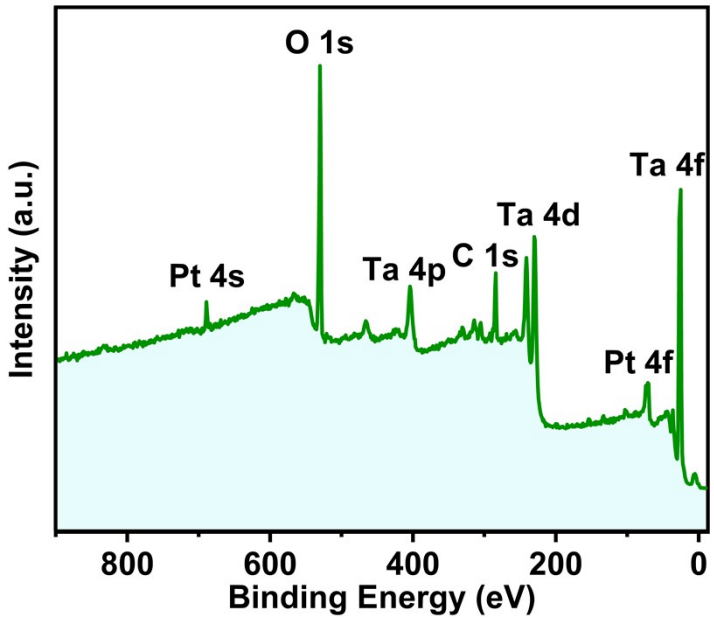

Fig. S3. XPS survey spectrum of 0.5Pt/Ta_2O_{5-x}.

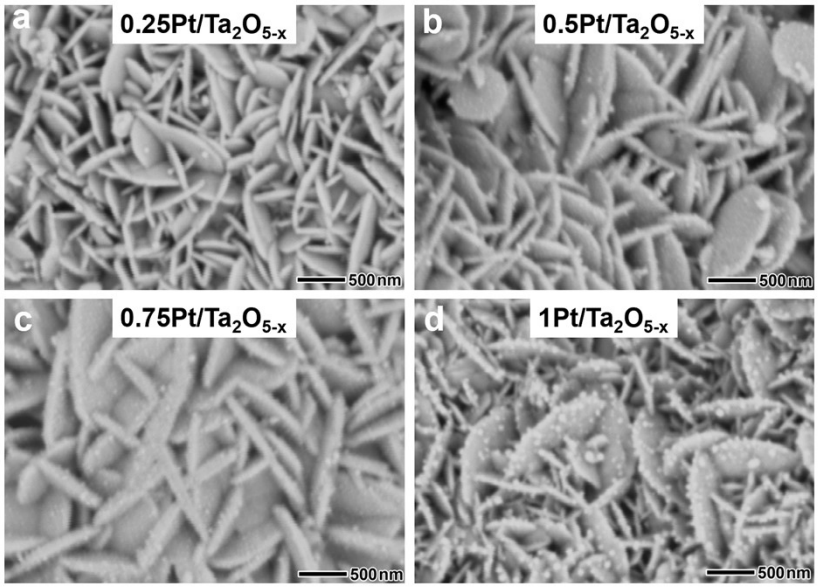

Fig. S4. SEM images of (a) 0.25Pt/Ta_2O_{5-x}, (b) 0.75Pt/Ta_2O_{5-x}, and (c) 1Pt/Ta_2O_{5-x}, respectively.

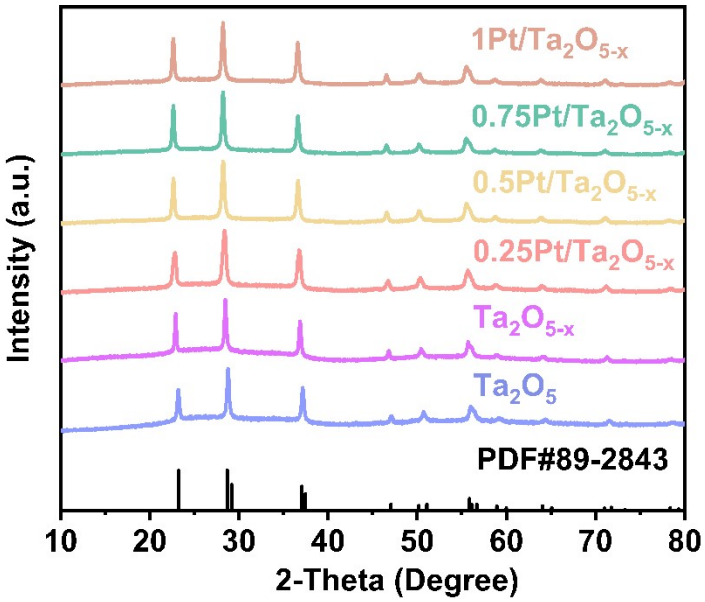

Fig. S5. XRD patterns of Ta_2O_5, Ta_2O_{5-x}, and Pt/Ta_2O_{5-x}, respectively.

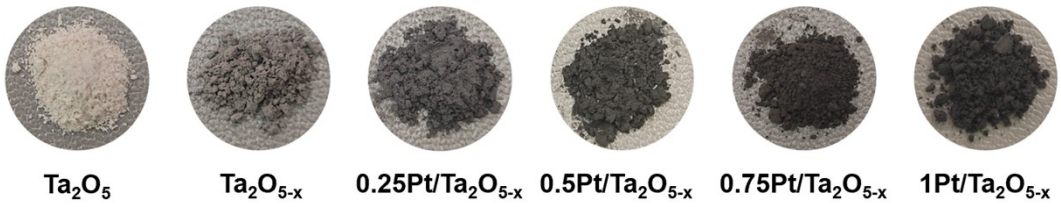

Fig. S6. Photographs of Ta_2O_5, Ta_2O_{5-x}, and Pt/Ta_2O_{5-x}, respectively.

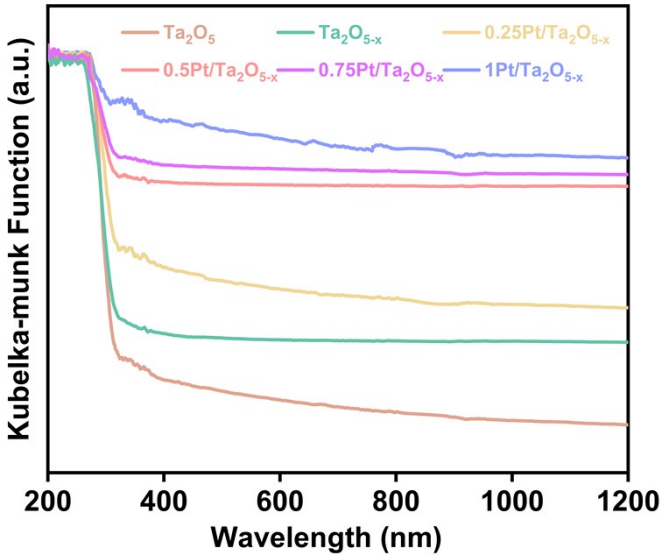

Fig. S7. UV−vis−NIR diffuse reflection spectra of Ta_2O_5, Ta_2O_{5-x}, and Pt/Ta_2O_{5-x}, respectively.

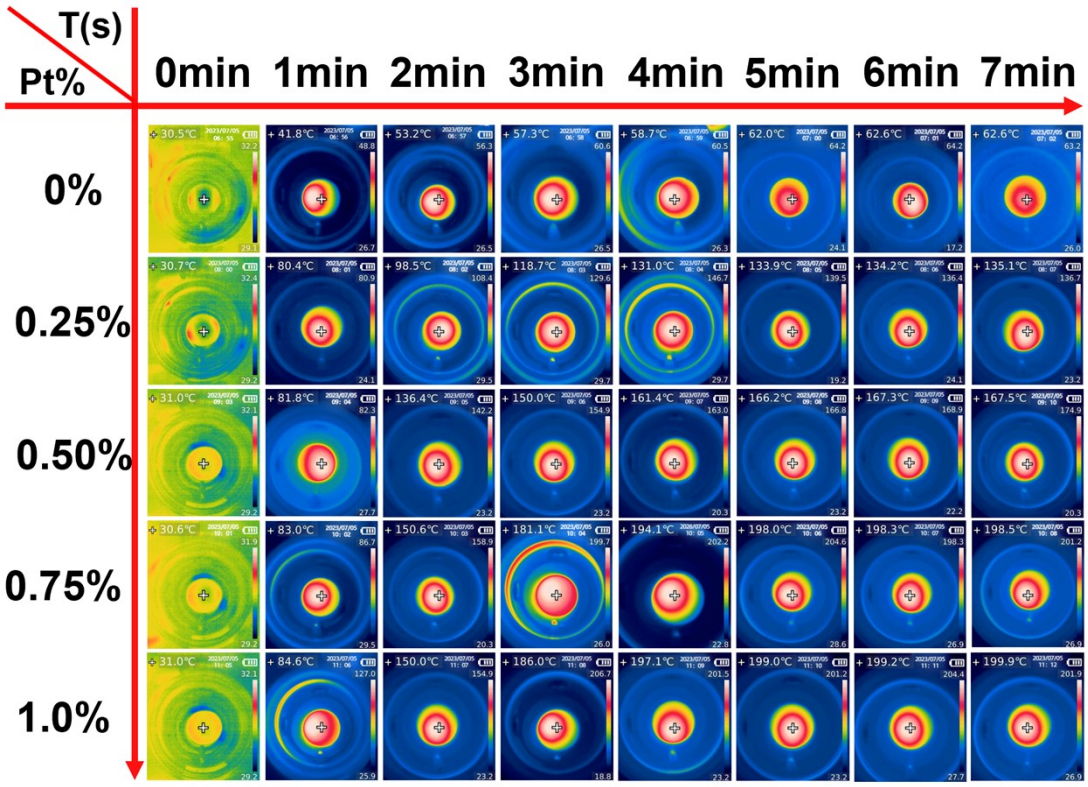

Fig. S8. Infrared photothermal images of Ta_2O_{5-x} and Pt/Ta_2O_{5-x} under continuous full-spectrum light irradiation (0.5 $W \cdot cm^{-2}$).

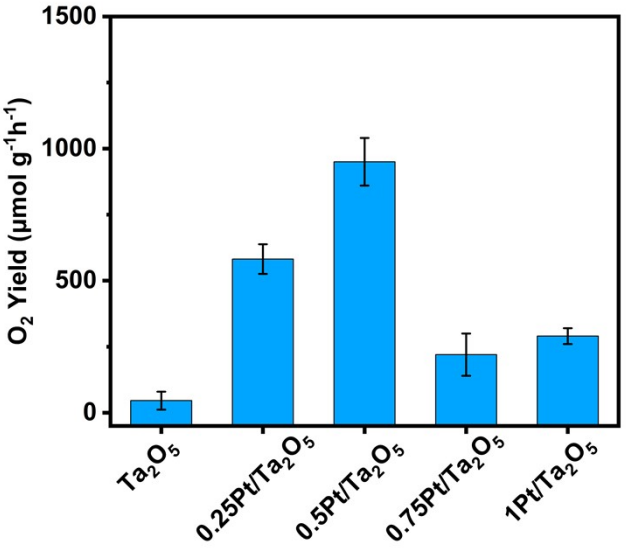

Fig. S9. O_2 yield rate over Ta_2O_5 and Pt/Ta_2O_5, respectively.

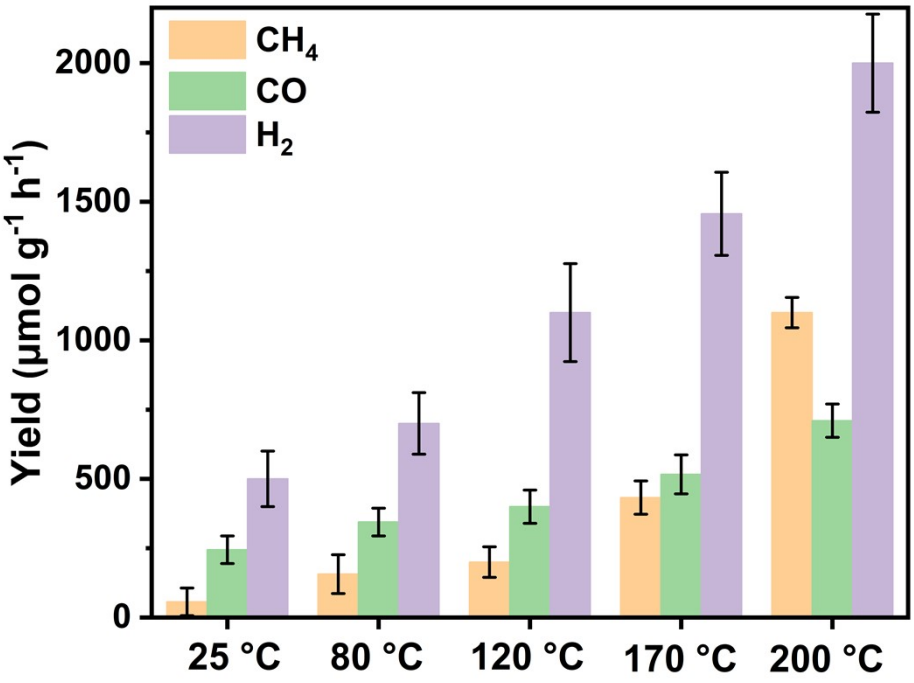

Fig. S10. The CO_2 reduction performance over $0.5Pt/Ta_2O_{5-x}$ system at different temperatures with the same irradiation intensity.

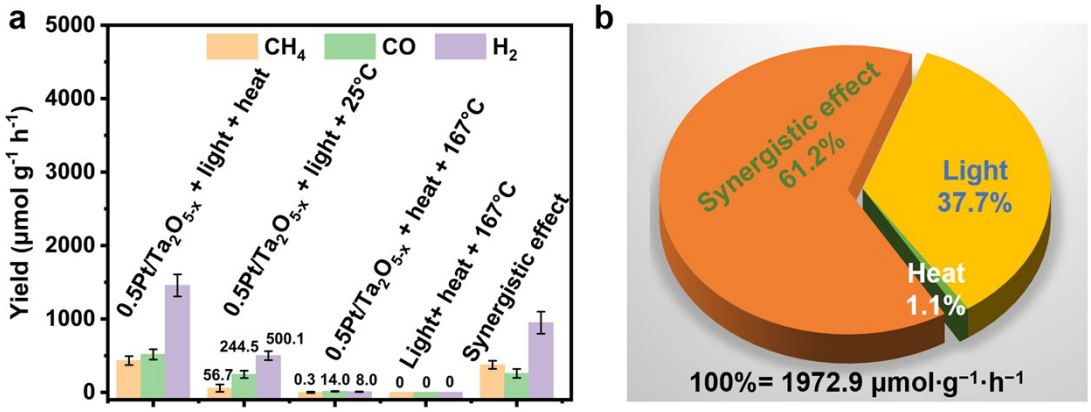

Fig. S11. (a) The CO_2 reduction performance over control variable catalysts. (b) Schematic diagram showing the respective percentage of light, heat, and synergy that contributed to the total syngas production.

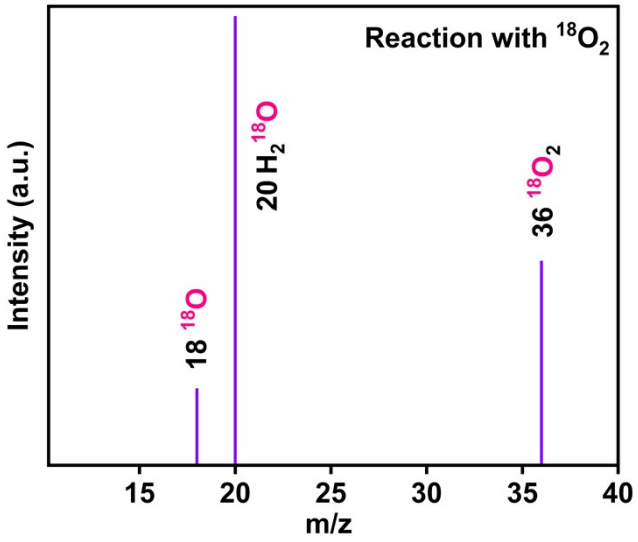

Fig. S12. Mass spectra of $^{18}O_2$ (m/z = 36) produced over $0.5Pt/Ta_2O_{5-x}$ in the photoreduction of $H_2{}^{18}O$.

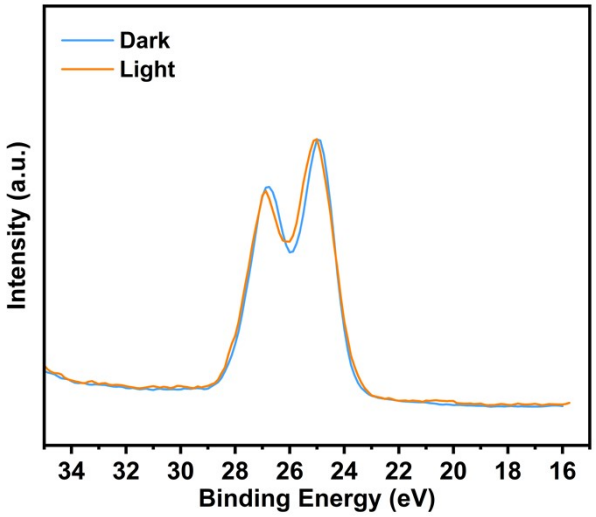

Fig. S13. Quasi in situ XPS spectra of Ta 4f for the Ta_2O_{5-x}.

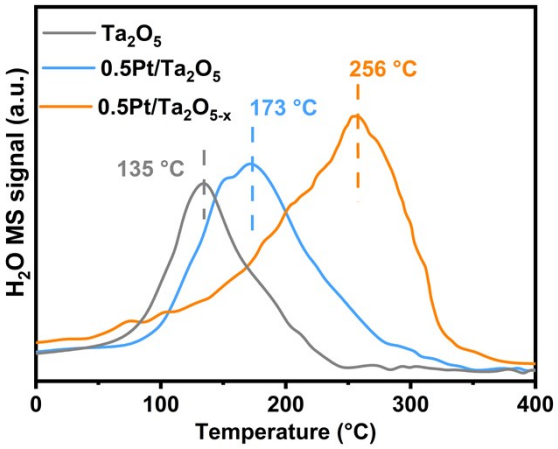

Fig. S14. The H_2O temperature-programmed desorption mass spectra of Ta_2O_5, Pt/Ta_2O_5, and Pt/Ta_2O_{5-x}, respectively.

.

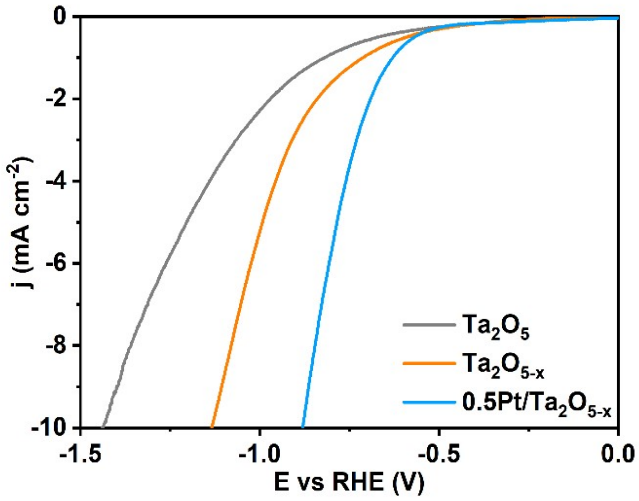

Fig. S15. Electrochemical linear sweep voltammetry curves with a scan rate of 5 mV s^{-1} in a CO_2-saturated 1.0 M NaOH solution.

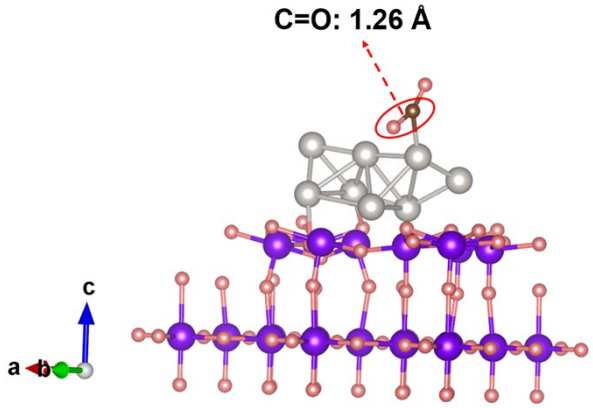

Fig. S16. The C=O bond length of CO_2 after adsorption on Pt/Ta_2O_{5-x}.

Table S1. Pt content in various Pt/Ta_2O_{5-x} catalysts measured by ICP.

Samples	Measured Pt/Ta (Mole ratio)
$0.25Pt/Ta_2O_{5-x}$	0.10%
$0.5Pt/Ta_2O_{5-x}$	0.19%
$0.75Pt/Ta_2O_{5-x}$	0.25%
$1Pt/Ta_2O_{5-x}$	0.38%

Table S2. Summary of the catalytic performance of the catalysts listed in Fig. 3e.

Catalyst	Light source	Reaction conditions	Metal loading	Major products	Product selectivity	AQY	Ref.
Pt/Ta_2O_{5-x}	300 W Xe lamp	Gas-solid, H_2O	0.5wt%	CO:516.4μmol g^{-1} h^{-1} H_2:1456.5μmol g^{-1} h^{-1} CH_4:432.6μmol g^{-1} h^{-1}	82% for syngas	3.5% (365nm)	This Work
$Cds/Pt/In_2O_3$	300 W Xe lamp with a 420 nm cut-off filter	H_2O, TEOA	1.97wt%	H_2:691μmol g^{-1} h^{-1} CH_4:383μmol g^{-1} h^{-1}	100% for CH_4	3.9% (420nm)	5
$Au\text{-}Pt/Cu_2O/ReS_2$	300 W Xe lamp	Gas-solid, H_2O	6.0wt%	CO:60.76μmol g^{-1} h^{-1} CH_4:39.45μmol g^{-1} h^{-1}	60% for CH_4	0.5% (420nm)	6
Co/C_3N_4	200mW Halogen lamps	MeCN, H_2O, TEOA	0.1wt%	CO:503μmol g^{-1} h^{-1}	71% for CO	0.4% (420nm)	7
Co/C_3N_4	300 W Xe lamp with a 420 nm cut-off filter	H_2O，TEOA，$C_{10}H_8N_2$，$CoCl_2$	0.12wt%	CO:37μmol g^{-1} h^{-1} H_2:6μmol g^{-1} h^{-1}	86% for CO	0.25% (420nm)	8
Co/Bi_3O_4Br	300 W Xe lamp	H_2O	0.8wt%	CO:107.1μmol g^{-1} h^{-1}	100% for CO	0.91% (380nm)	9
Co/C_3N_4	300 W Xe lamp with a 400 nm cut-off filter	MeCN, H_2O, TEOA	4.4wt%	CO:17μmol g^{-1} h^{-1} CH_4:0.7μmol g^{-1} h^{-1}	80% for CO	0.8% (420nm)	10
Ru/ZnS	150 W XBO arc lamp with a 320 nm cut-off filter	H_2O，C_3H_8O	0.1wt%	CO:84μmol g^{-1} h^{-1} HCOOH:240μmol g^{-1} h^{-1}	74% for HCOOH	0.5% (375nm)	11
Ru/Ta_2O_5	300 W Xe lamp	MeCN, H_2O, TEOA	1.0wt%	HCOOH :7μmol g^{-1} h^{-1}	75% for HCOOH	1.9% (405nm)	12
Ru/C_3N_4	400 W High-pressure mercury lamps	$K_2C_2O_4{\cdot}H_2O$，EDTA·2Na，H_2O	5.0wt%	HCOOH:42.3μmol g^{-1} h^{-1}	98% for HCOOH	5.2% (400nm)	13
Ru/GaN:ZnO	300 W Xe lamp with a 400 nm cut-off filter	Na_2CO_3，H_2O，Na_4EDTA	1.5wt%	H_2:30μmol g^{-1} h^{-1} HCOOH:65μmol g^{-1} h^{-1}	68% for HCOOH	1% (400nm)	14
Ag/CN	300 W Xe lamp with a 400 nm cut-off filter	Gas-solid, H_2O	0.73wt%	CO:160μmol g^{-1} h^{-1}	94% for CO	4.8% (365nm)	15
$Al@Cu_2O$	300 W Xe lamp with a 400 nm cut-off filter	CO_2，H_2	5.0wt%	CO:360 μmol$cm^{-2}h^{-1}$	97% for CO	0.35% (420nm)	16
Au/TZO	300 W Xe lamp with a 400 nm cut-off filter	MeCN, H_2O, TEOA	1.2wt%	H_2:271.6μmol g^{-1} h^{-1} CO:260.6μmol g^{-1} h^{-1}	98% for syngas	2.4% (400nm)	17
CuO/TiO_2	40 W Hg UV lamp	Gas-solid, H_2O	3.0wt%	CO:14.5μmol g^{-1} h^{-1} H_2:2.8μmol g^{-1} h^{-1} CH_4:2.1μmol g^{-1} h^{-1}	75% for CO	2% (254nm)	18

REFERENCES

1. Delley, B. An all-electron numerical method for solving the local density functional for polyatomic molecules. *J. Chem. Phys*. **1990**, 92, 508–517.

2. Delley, B. From molecules to solids with the DMol3 approach. *J. Chem. Phys*. **2000**, 113, 7756–7764.

3. Kresse, G., Furthmu¨ller, J. Efficient iterative schemes for ab initio total-energy calculations using a plane-wave basis set. *Phys. Rev. B Condens. Matter*. **1996**, 54, 11169–11186.

4. Perdew, J. P., Burke, K., Ernzerhof, M. Generalized gradient approximation made simple. *Phys. Rev. Lett*. **1996**, 77, 3865.

5. Liu, P.; Men, Y. L.; Meng, X. Y.; Peng, C.; Zhao, Y.; Pan, Y. X., Electronic Interactions on Platinum/(Metal-Oxide)-Based Photocatalysts Boost Selective Photoreduction of CO_2 to CH_4. *Angew. Chem. Int. Ed.* **2023,** 62, e202309443.

6. Zeng, J.; Jiang, Z.; Lv, K.; Ahmad, SA.; Chen, X.; Zhang, W.; J.; Zhu, T., Experimental and calculation investigations of the photocatalytic selective and performance for CO_2 reduction by cobalt-doped $Bi_4O_5Br_2$ nanosheets. *Ceram. Int.* **2024,** 12.

7. Huang, P.; Huang, J.; Pantovich, S. A.; Carl, A. D.; Fenton, T. G.; Caputo, C. A.; Grimm, R. L.; Frenkel, A. I.; Li, G., Selective CO_2 reduction catalyzed by single cobalt sites on carbon nitride under visible-light irradiation. *J. Am. Chem. Soc.* **2018,** 140, 16042-16047.

8. Lin, J.; Pan, Z.; Wang, X., Photochemical reduction of CO_2 by graphitic carbon nitride polymers. *ACS Sustain. Chem. Eng.* **2014,** 2, 353-358.

9. Di, J.; Chen, C.; Yang, S. Z.; Chen, S.; Duan, M.; Xiong, J.; Zhu, C.; Long, R.; Hao, W.; Chi, Z.; Chen, H., Isolated single atom cobalt in Bi_3O_4Br atomic layers to trigger efficient CO_2 photoreduction. *Nat. Commun.* **2019,** 10, 2840.

10. Zhao, G.; Pang, H.; Liu, G.; Li, P.; Liu, H.; Zhang, H.; Shi, L.; Ye, J., Co-porphyrin/carbon nitride hybrids for improved photocatalytic CO_2 reduction under visible light. *Appl. Catal. B: Environ.* **2017,** 200, 141-149.

11. Baran, T.; Wojtyła, S.; Dibenedetto, A.; Aresta, M.; Macyk, W., Zinc sulfide functionalized with ruthenium nanoparticles for photocatalytic reduction of CO_2. *Appl. Catal. B: Environ.* **2015,** 178, 170-176.

12. Sato, S.; Morikawa, T.; Saeki, S.; Kajino, T.; Motohiro, T., Visible-Light-Induced Selective CO_2 Reduction Utilizing a Ruthenium Complex Electrocatalyst Linked to a p-Type Nitrogen-Doped Ta_2O_5 Semiconductor. *Angew. Chem. Int. Ed.* **2010,** 4, 5101.

13. Kuriki, R.; Matsunaga, H.; Nakashima, T.; Wada, K.; Yamakata, A.; Ishitani, O.; Maeda, K., Nature-inspired, highly durable CO_2 reduction system consisting of a binuclear ruthenium (II) complex and an organic semiconductor using visible light. *J. Am. Chem. Soc.* **2016,** 138, 5159-5170.

14. Nakada, A.; Kuriki, R.; Sekizawa, K.; Nishioka, S.; Vequizo, J. J. M.; Uchiyama, T.; Kawakami, N.; Lu, D.; Yamakata, A.; Uchimoto, Y.; Ishitani, O., Effects of interfacial electron transfer in metal complex–semiconductor hybrid photocatalysts on Z-scheme CO_2 reduction under visible light. *ACS Catal.* **2018,** 8, 9744-9754.

15. Hu, S.; Qiao, P.; Yi, X.; Lei, Y.; Hu, H.; Ye, J.; Wang, D., Selective photocatalytic reduction of CO_2 to CO mediated by silver single atoms anchored on tubular carbon nitride. *Angew. Chem. Int. Ed.* **2023,** 62, e202304585.

16. Robatjazi, H.; Zhao, H.; Swearer, D. F.; Hogan, N. J.; Zhou, L.; Alabastri, A.; McClain, M. J.; Nordlander, P.; Halas, N. J., Plasmon-induced selective carbon dioxide conversion on earth-abundant aluminum-cuprous oxide antenna-reactor nanoparticles. *Nat. Commun.* **2017,** 8, 27.

17. Huang, N. Y.; Li, B.; Wu, D.; Chen, Z. Y.; Shao, B.; Chen, D.; Zheng, Y. T.; Wang, W.; Yang, C.; Gu, M.; Li, L., Crystal Engineering of MOF-Derived Bimetallic Oxide Solid Solution Anchored with Au Nanoparticles for Photocatalytic CO_2 Reduction to Syngas and C_2 Hydrocarbons. *Angew. Chem. Int. Ed.* **2024,** e202319177.

18. Fang, B.; Xing, Y.; Bonakdarpour, A.; Zhang, S.; Wilkinson, D. P., Hierarchical CuO–TiO_2 hollow microspheres for highly efficient photodriven reduction of CO_2 to CH_4. *ACS Sustain. Chem. Eng.* **2015,** 3, 2381-2388.